Atomic and electronic structure of amorphous and crystalline hafnium oxide: X-ray photoelectron spectroscopy and density functional calculations

T. V. Perevalov and V. A. Gritsenko[a)]
Institute of Semiconductor Physics, Novosibirsk 630090, Russia

S. B. Erenburg and A. M. Badalyan
Institute of Inorganic Chemistry, Novosibirsk 630090, Russia

Hei Wong[b)]
Department of Electronic Engineering, City University of Hong Kong, Tat Chee Avenue, Hong Kong

C. W. Kim
Samsung Advanced Institute of Technology, P.O. Box 111, Suwon 440-600, Korea

(Received 21 August 2006; accepted 21 December 2006; published online 7 March 2007)

The atomic structure of amorphous and crystalline hafnium oxide (HfO_2) films was examined using x-ray diffractometry and Hf edge x-ray absorption spectroscopy. According to the x-ray photoelectron spectroscopy and band data calculated by the density functional method, we found that the valence band of HfO_2 consists of three subbands separated by ionic gaps. The upper subband is formed by O $2p$, Hf $4f$, and Hf $5d$ states; the intermediate subband is formed by O $2s$ and Hf $4f$ states, whereas the lower narrow subband is mainly formed by Hf $5p$ states. The energy gap of amorphous HfO_2 is 5.7 eV as determined by electron energy loss spectroscopy. The band calculation results indicate the existence of light ($0.3m_0$) and heavy ($8.3m_0$) holes in the HfO_2 film and the effective mass of electron lies in the interval of $0.7m_0-2.0m_0$. © *2007 American Institute of Physics*. [DOI: 10.1063/1.2464184]

I. INTRODUCTION

It is well known that the key dielectrics for manufacturing the silicon devices are amorphous silicon dioxide (a-SiO_2) and amorphous silicon nitride (a-Si_3N_4). After 40 years of intensive study, the atomic and electronic properties of these dielectrics are now well understood.[1–3] As the thicknesses of the silicon oxide and silicon nitride are being scaled down to their physical limits, a pressing problem in modern microelectronics is to replace the conventional dielectrics by high dielectric permittivity (high-k) ones.[3–9] This alternative can help solving the related problem of high leakage currents across ultrathin (~10 Å) SiO_2 layers in metal-oxide-semiconductor (MOS) structures.[5]

In dynamic random access memory (DRAM) technology, the use of high-k dielectrics can make the charge storage area smaller so as to increase the memory capacity.[10,11] The high-k dielectrics also offer a unique feature for improving the operation of flash-memory devices. It enhances the rewrite speed and charge storage duration and reduces the programming (write/erase) voltages.[10,11] Numerous high-k dielectric materials have been studied intensively. Hafnium dioxide (HfO_2) with dielectric constant of about 25 is considered as one of the most promising candidates.[5,8]

Under normal pressure, single-crystal HfO_2 is available in three polymorphic modifications: a low-temperature monoclinic phase (space group $P2_1/c$), a tetragonal phase (space group $P4_2/nmc$) obtained at temperatures above 2000 K, and the cubic phase ($Fm3m$) that forms at temperatures above 2870 K.[12,13] In the cubic and tetragonal phases, the oxygen is fourfold coordinated, and the Hf atom is eightfold coordinated. In the monoclinic phase, the coordination numbers for O atoms can be either three- or fourfold, and the Hf atoms can be seven- or eightfold coordinated.

At room temperatures, crystalline HfO_2 exists in the monoclinic modification. A cubic modification was observed at 200 °C in thin HfO_2 and ZrO_2 films with thicknesses ranging from 100 to 500 Å.[14–17] In the temperature range of 300–600 °C, films with thicknesses between 100 and 500 Å are a tetragonal modification of HfO_2, with parameters substantially differing from the high-temperature bulk modification.[14,17] Stable monoclinic phase is normally observed in films thicker than 500 Å.

The electronic structure of HfO_2 in its cubic, tetragonal, and monoclinic modifications was theoretically examined by Demkov.[18] This author found that the valence band of HfO_2 is made up of two subbands. However, the band gap energy predicted by numerical calculations turned out to be substantially smaller than its experimental value. A theoretical study of the density of electronic states in the monoclinic modification of HfO_2 was also reported by Foster *et al.*[19] This study is important for investigating the charge transport through such thin films. Suppression of leakage currents across the gate dielectrics of MOS structures is currently the crucial issue. The large electric field across the thin dielectric film makes the direct and Fowler-Nordheim tunneling through the Si/dielectric energy barrier possible. The injection current exponentially depends on the *effective mass* m^* of the tunneling charge carriers in the dielectric.[20,21] Band calculation and experimental data show that in SiO_2 and Si_3N_4 there

[a)]Also at Semiconductor Physics Department, Tomsk State University.
[b)]Electronic mail: eehwong@cityu.edu.hk

exist "light" electrons with effective mass in the range of $0.3m_0-1.4m_0$ and heavy holes with effective mass in the range of $2.5m_0-10m_0$.[21–25] The heavy holes in these materials are due to the narrow band formed by the antibonding O $2p_\pi$ and N $2p_\pi$ orbitals in SiO_2 and Si_3N_4, respectively. Neither theoretical nor experimental study on the effective electron or hole mass in HfO_2 has been reported so far. The purposes of the present study is to examine, both experimentally and theoretically, the atomic and electronic structure of HfO_2, and to use these results in estimating the effective electron and hole masses in this material.

II. EXPERIMENT

The starting materials were ⟨100⟩-oriented *n*-Si substrates with resistivity of 20 Ω cm. Prior to the deposition, the Si substrates were cleaned with the standard RCA procedure. HfO_2 films with thicknesses in the range of 200–600 Å were then deposited onto the wafers using an ARC-12M sputter, with a purity of 99% hafnium target. Note that the objective of this work is to study the bulk properties of HfO_2 and the density function calculations to be presented later are also focused on the bulk structure. To minimize the interface effects, the films prepared in this work are much thicker than those used in the current MOS devices for electrical properties characteristics. The vacuum chamber was pumped down to a pressure of 10^{-6} Torr and then subsequently filled with an oxygen/argon mixture. The argon-to-oxygen flow ratio was 2:23. During the deposition of the HfO_2 films, the pressure in the chamber was maintained at a level of 10^{-3} Torr and the substrate temperature was 150 °C. The as-deposited films using this method are amorphous. The chemical composition and the stoichiometry were studied with x-ray photoelectron spectroscopy (XPS) measurement. The as-deposited film is slightly oxygen deficient.[8] Part of the samples was further annealed at 800 °C in atmosphere for 30 min in order to improve the film stoichiometry and to have significant crystallization effects for the easy of experimental investigation. Lower annealing temperature and shorter duration may be adopted to minimize the crystallization effects, but the microcrystallites should still have notable effect as the crystallization phase can be found at processing temperature of 325 °C for sample being prepared using atomic layer deposition (ALD) method.[5]

Various characterizations were conducted for the samples. X-ray phase analysis (XPA) was conducted by studying the diffraction of synchrotron radiation with wavelength λ=1.5406 Å. X-ray diffraction patterns were registered on a high-resolution diffractometer in the Institute of Nuclear Physics at Novosibirsk. A glancing incidence scheme with $\theta\approx4°$ was used. The sample was rotated around the normal to the film surface. The x-ray diffraction patterns were recorded at a scanning pitch of $\Delta(2\theta)=0.05°$ with the interval (2θ) in the range of 20°–70°.

Edge x-ray absorption fine spectra (EXAFS) measurements of the HfO_2 films were conducted to study the fine structure of the Hf *K* near-edge absorption. These characteristics were measured using the synchrotron radiation produced by the VEPP-3 storage ring (also in Institute of Nuclear Physics, Novosibirsk) with energy of 2 GeV and current ranging from 50 to 100 mA. The radiation detector was a gamma ionization chamber filled with Ar/He mixture and a double-crystal monochromator (a ⟨111⟩-oriented split Si single crystal) was used in the detector. The EXAFS spectra were registered using the surface-sensitive fluorescent technique. By measuring the intensity of the secondary (fluorescent) radiation emitted by a decaying "hole" state of an atom where a deep vacancy was generated by gamma-quantum absorption, the x-ray absorption coefficient can be determined. To eliminate the reflections of the synchrotron radiation from the substrate, the sample was mounted on a turning table rotated with frequencies in the range of 10–15 Hz. Phase and amplitude characteristics of the EXAFS data were calculated through the $X\alpha$-DW (Debye-Waller factor) approximation using the EXCURV92 package.[26] To analyze the local atomic environment, a fitting procedure with *k* weighting was applied to the Fourier-filtered data to yield the dependences $k\chi(k)$, where $\chi(k)$ is the normalized oscillating absorption coefficient and *k* is the wave number. The fitting was performed in the interval of photoelectron wave vectors from 3 to 12 $Å^{-1}$.

X-ray and ultraviolet photoelectron spectra were measured using a VG ESCALAB 220i-XL spectrometer with an Al $K\alpha$ monochromatic radiation source with energy of 1486.6 eV or helium plasma with energy of 21.2 eV (He I) or 40.8 eV (He II).

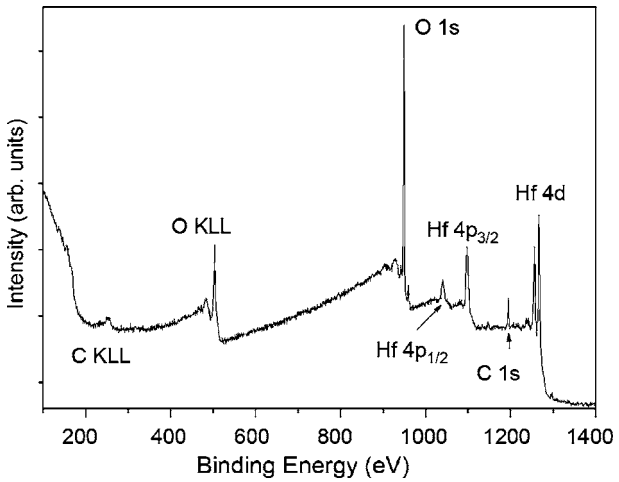

FIG. 1. Survey of x-ray photoelectron spectrum for amorphous HfO_2.

III. RESULTS AND DISCUSSIONS

A. Atomic structure of HfO_2 films

Figure 1 shows a survey of the x-ray photoelectron spectrum on an amorphous HfO_2 film. Estimations from the ratio of Hf 4*d* and O 1*s* peak intensities confirm that the chemical composition of this film is essentially stoichiometric. Figure 2 shows the x-ray diffraction patterns for as-deposited and annealed (800 °C for 30 min in ambient air) HfO_2 films. Compared with the x-ray diffraction (XRD) pattern of monoclinic HfO_2 powder (plotted in squares in the bottom picture), it suggests that the annealed HfO_2 films are crystalline (with a monoclinic structure and a lattice parameter *a*

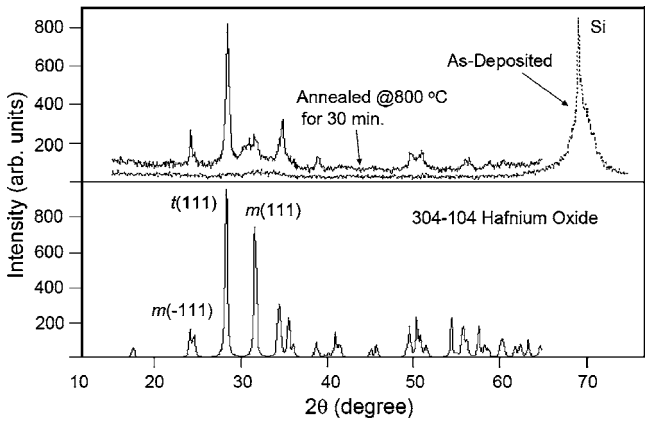

FIG. 2. X-ray diffraction patterns of Hf films: 1—as-deposited film and 2—film annealed at 800 °C for 30 min (upper figure). Comparison with an x-ray diffraction pattern taken from powdered monoclinic HfO_2 (lower figure).

=5.08 Å). The formation of the monoclinic structure during the 800 °C annealing can be explained by the existence of a thermodynamically nonequilibrium amorphous modification of HfO_2 in the initial state.

Figure 3 shows the modulus of the Fourier transform of the function $k^2\chi(k)$ extracted from the Hf *K* EXAFS spectrum (radial structural functions without phase corrections) for a HfO_2 film, before and after thermal annealing. It indicates that the as-deposited films are completely amorphous as there is no detectable Hf–Hf separation. The annealed sample results in a rise in the Hf–O amplitude in the first coordination sphere of the metal atoms (ordering) and gives rise to a Hf–Hf peak and to peaks corresponding to the ordered arrangement of oxygen atoms in the farther coordination spheres of Hf (see Fig. 3, curve 2).

B. Electronic structure of amorphous HfO_2 films

Figure 4 shows an ultraviolet photoelectron spectrum due to the valence band of amorphous HfO_2 measured at an

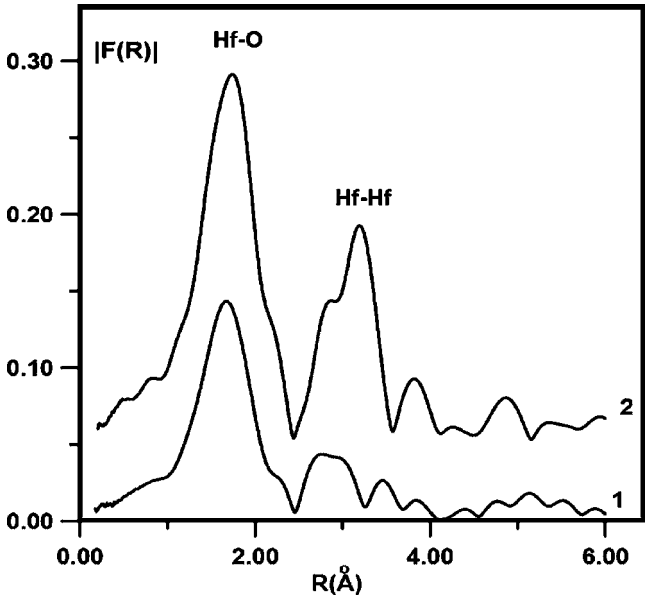

FIG. 3. Radial distribution function as extracted from Hf *K* near-edge absorption spectra: 1—as-deposited HfO_2 film and 2—HfO_2 film annealed at 800 °C for 30 min.

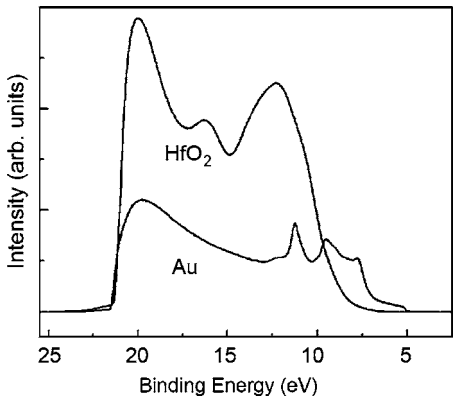

FIG. 4. Ultraviolet photoelectron spectra of amorphous HfO_2 and Au excited by He I radiation with energy of 21.2 eV.

excitation energy of 21.2 eV. Also shown in the same figure is the Au spectrum to be used as a reference for determining the valence band level.

The low-energy part of the spectrum controls the energy position of the top of the valence band in amorphous HfO_2. As the Au work function (Fermi-level position with respect to the vacuum level) is 5 eV and the top of the valence band of amorphous HfO_2 is about 1.5 eV above the Au Fermi level, the top of the HfO_2 valence band (E_V) is 6.5 eV lower than the vacuum level. Since the energy position of the Au Fermi level coincides with the top of Si valence band, E_V(Si), the height of the energy barrier for hole injection from Si into amorphous HfO_2 thus amounts to 1.5 eV also.

The width of the energy gap in amorphous HfO_2 was estimated from electron energy loss spectroscopy (EELS) data obtained with a 200 eV monochromatic electron beam (see Fig. 5). The zero energy in the figure refers to the position of the peak due to elastically reflected electrons. Negative energies refer to inelastically reflected electrons. The width of the forbidden gap (E_g) in amorphous HfO_2 as extracted from Fig. 5 is in the range of 5.7±0.3 eV. This value agrees with other reports.[27,28]

The solid curve in Fig. 6 is an experimental XPS spectrum due to the valence band of amorphous HfO_2. The dotted curve in this figure represents a Gaussian fit of the full density of valence band states predicted with allowance for the ionization cross sections of the 5*p*, 4*f*, 5*d*, and 6*s* orbitals of

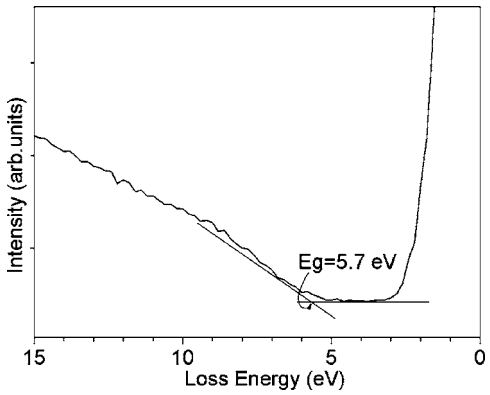

FIG. 5. Electron energy loss spectra of amorphous HfO_2. The zero energy refers to the peak due to elastically reflected electrons.

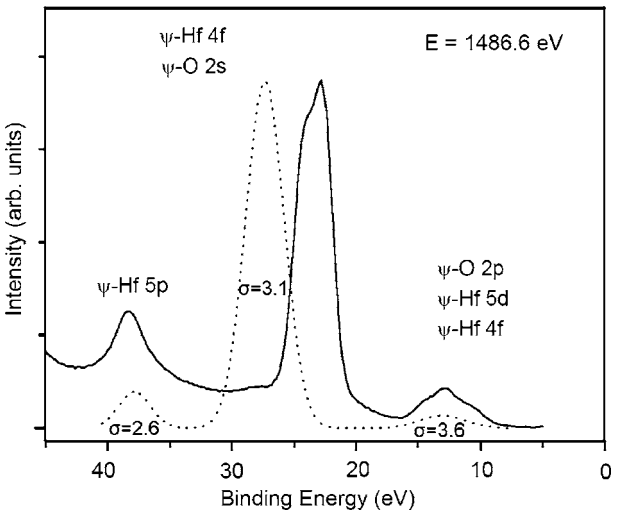

FIG. 6. An x-ray photoelectron spectrum of amorphous HfO_2 taken at an excitation energy of 1486.6 eV (solid curve) and the predicted photoionization cross section (dashed curve).

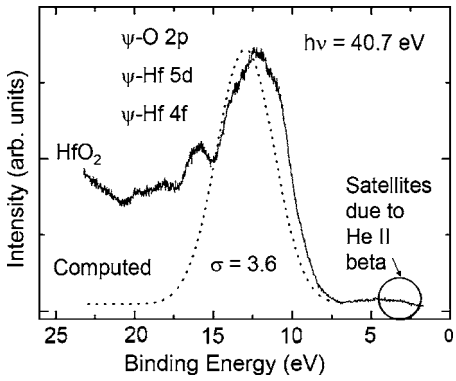

FIG. 7. The photoelectron spectrum of amorphous HfO_2 measured with excitation energy of 40.8 eV and the predicted density of states in the valence band were normalized with the photoionization cross section.

Hf and $2p$ and $2s$ orbitals of O. The values of the ionization cross sections are listed in Table I. The dispersion in each peak is assumed to be equal to the width at half-height of the corresponding peak in the experimental curve. The valence band of HfO_2 is split into three subbands with roughly identical widths at half-height of 3 eV. The prevailing contribution to the spectrum is due to the $4f$, $5d$, and $5p$ states of Hf and due to the $2p$ and $2s$ states of oxygen. An ultraviolet photoelectron spectrum of amorphous HfO_2 taken at an excitation energy of 40.8 eV is shown in Fig. 7. The prevailing contribution to the experimental spectrum is made by O $2s$ states.[30]

C. Electronic structure of the three crystalline modifications

To construct the band diagrams of the cubic, tetragonal, and monoclinic modifications of HfO_2 and to determine the effective masses of holes and electrons in these crystals, quantum-mechanical calculation using the Amsterdam density functional (ADF) BAND program was conducted. The ADF program was used to calculate the electronic structure of atoms and molecules, and BAND is a subprogram in the ADF package for calculating periodic atomic systems (atomic chains and layers, and bulk crystals).[31–33] The program is based on the theory of the Kon-Shem density functional in the local-density approximation for the exchange and correlation energies. The program calculates the electron density and total energy of multielectron systems. It allows the user to reconstruct the band structure, to predict the total density of states (TDOS) and the partial densities of states (PDOS) for all spherical harmonics with a certain value l of the orbital momentum, and to analyze the charges at the atoms in the system.

The crystal structures and the respective Brillouin zones with singular points are shown in Fig. 8. In the cubic modification of HfO_2, the Bravais lattice is a face-centered-cubic lattice, and the unit cell is the primitive rhombohedric cell. The translation vectors are $(a/2,a/2,0)$, $(a/2,0,a/2)$, and $(0,a/2,a/2)$, and the lattice constant is $a=5.08$ Å.[29] The basis is formed by three atoms: one Hf atom is located at (0, 0, 0) and two O atoms are located at $(a/4,a/4,-a/4)$ and $(a/4,a/4,a/4)$.

In the tetragonal modification of HfO_2 the unit cell is a regular prism with squared basis. The translation vectors are $(a,0,0)$, $(0,a,0)$, and $(0,0,c)$, where $a=3.56$ Å and $c=5.11$ Å.[29] The structure of the tetragonal HfO_2 readily forms from the cubic phase of HfO_2: in the $\langle 001 \rangle$ direction, the lattice constant increases to $c=5.11$ Å, and the oxygen columns shift by $\delta=0.19$ Å, while the neighboring columns experiencing antiphase shifts. The basis consists of six atoms: two Hf atoms are located at (0, 0, 0) and $(a/2,a/2,c/2)$ and four O atoms are located at $(a/2,0,c/4-\delta)$, $(a/2,0,-c/4-\delta)$, $(0,a/2,c/4+\delta)$, and $(0,a/2,-c/4+\delta)$.

The space lattice of the monoclinic modification of HfO_2 has primitive unit cell with the translation vectors $(a,0,0)$, $(0,b,0,)$, and $(c\cos\gamma,0,c\sin\gamma)$, where $a=5.08$ Å, $b=5.19$ Å, $c=5.22$ Å, and $\gamma=99.77$.[29,31] The basis consists of 12 atoms whose coordinates are listed in Table II. The unit cell of the monoclinic modification of HfO_2 involves two types of oxygen atoms, one (O1) is three-coordinated and the other (O2) is four coordinated.

TABLE I. Photoionization cross-section coefficients for the $5p$, $4f$, $5d$, and $6s$ orbitals of Hf and for $2p$ and $2s$ orbitals of O.

	Hf				O	
$\hbar\omega$ (eV)	$5p$	$4f$	$5d$	$6s$	$2s$	$2p$
40.8	7.9990	0.9905	2.5980	0.0755	0.8342	6.8160
1486.6	0.1014	0.1108	0.0245	0.0005	0.0190	0.0003

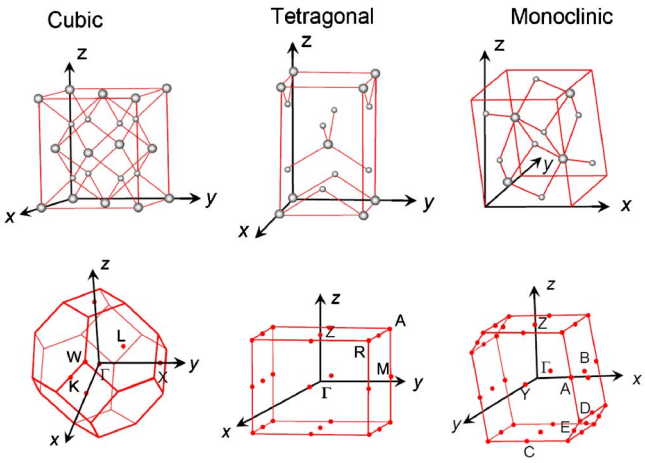

FIG. 8. Crystal structures and their respective Brillouin zones for the crystalline phases of HfO_2.

In computing the electronic structure of the cubic, tetragonal, and monoclinic crystalline modifications of HfO_2 with ADF and BAND programs, the Bloch electron functions in the crystal are sought in the form of an expansion in basis functions. For the basis functions, two types of functions are used: numerical orbitals (NO) and Slater orbitals (STO). The numerical orbitals are the wave functions predicted by the Herman-Skilman program, and the Slater orbitals are

$$X_{n,l,m} = Ar^{\acute{n}-1} \exp(-\xi r) Y_{lm}, \quad (1)$$

where $\acute{n}$ is the effective principal quantum number. Combination of NO and STO in the basis set imparts the set with a high variational flexibility that guarantees a good accuracy of the calculations with a comparatively limited number of basis functions. The molecular orbital is calculated by only involving the atomic orbital due to the valence electrons and the inner atomic shells are frozen.

The number of basis functions per unit cell in the cubic modification of HfO_2 is 75, and the values of cell numbers for the tetragonal and monoclinic configurations are 150 and 300, respectively. Integration over the Brillouin zone was performed with 65, 75, and 119 k points in the irreducible part of the Brillouin zone for the cubic, tetragonal, and monoclinic modifications, respectively. Similar calculations for the band structure of the cubic, tetragonal, and monoclinic modifications of HfO_2, but with a basis set made up by plane waves were reported previously by Holgado *et al.*[14]

TABLE II. Positions of the basis atoms in the primitive cell of monoclinic HfO_2 (Cartesian coordinate system).

	X (Å)	Y (Å)	Z (Å)
	0	0	0
Hf	2.4761	0.4516	2.1444
atoms	2.9189	2.5951	0.4278
	0.4429	2.1434	2.5722
	1.1366	1.5898	0.6349
	1.3395	2.0414	2.7793
	1.7824	4.1848	0.2071
O	1.5795	0.5536	3.2071
atoms	0.5968	3.7156	1.4201
	3.0729	4.1673	3.5644
	3.5158	6.3106	0.9923
	0.1539	1.5723	3.9922

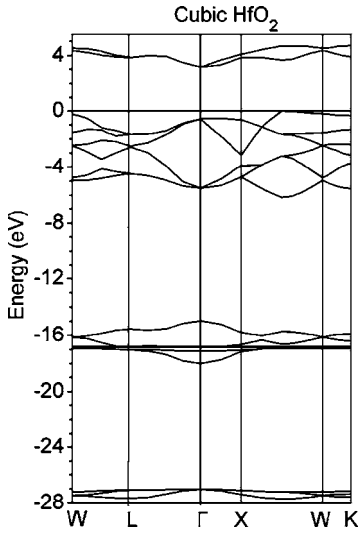

FIG. 9. E-k diagram across the singular points of Brillouin zone for cubic HfO_2.

Figures 9–11 show the theoretically predicted band diagrams of the cubic, tetragonal, and monoclinic crystalline modifications of HfO_2 drawn through the Brillouin zone singular points (see Fig. 8). Here and below, the zero energy is taken to coincide with the top of the valence band. With enlarged atomic basis, the band structure becomes more complicated, although having a similar appearance for all the three modifications. It can be concluded from the present results that the properties of HfO_2 are defined by the short range and not by the long-range atomic ordering.

In the cubic modification of HfO_2, the valence band top E_V lies at the point X of the Brillouin zone, and the conduction-band bottom E_C at the point Γ. The band gap energy in the cubic modification of HfO_2 can be estimated as

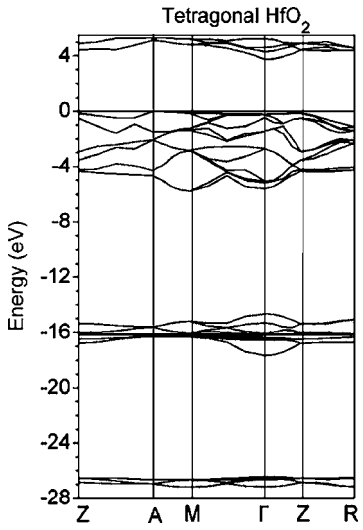

FIG. 10. E-k diagram across the singular points of Brillouin zone for tetragonal HfO_2.

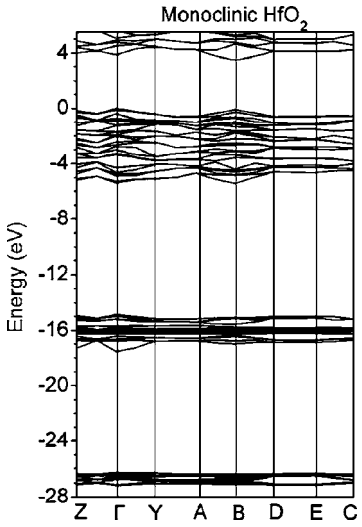

FIG. 11. *E-k* diagram across the singular points of Brillouin zone for monoclinic HfO_2.

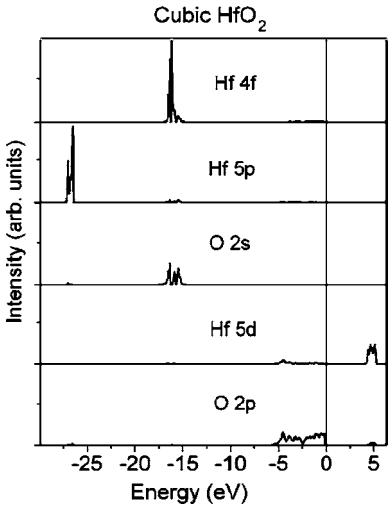

FIG. 12. Partial densities of the states due to $4f$, $5p$, and $5d$ orbitals of Hf and of those due to $2s$ and $2p$ orbitals of O in cubic HfO_2.

the difference between the valence band top and the conduction band bottom and is $E_g=E_C-E_V=3.2$ eV. In the tetragonal modification, E_V and E_C lie at the Γ and M points of the Brillouin zone, respectively, giving $E_g=3.8$ eV. For the monoclinic modification, E_V lies at the Γ point of the Brillouin zone and E_C at the B point, giving $E_g=3.5$ eV. Thus, all the three modifications of HfO_2 are indirect band gap dielectrics, and the band gap energies E_g are approximately in the range of 3.2–3.8 eV. These values are significantly less than the experimental values (in the range of 5.3–5.8 eV, according to various authors).[27,28] This discrepancy can be attributed to the fact that density functional theory (DFT) calculations normally yield an underestimated value for the band gap energy.

The effective masses of electrons and holes (see Table III) were calculated using a square approximation of the $E(\mathbf{k})$ dispersion curves near the edges of the valence and conduction bands, i.e.,

$$m^* = \frac{\Delta k^2}{2\Delta E}, \tag{2}$$

where ΔE is the energy difference between the minimum and maximum energies at the points lying apart at the distance Δk in the inverse space in the corresponding direction.

Calculations show that in each crystalline modification of HfO_2, there exist heavy as well as light holes, the effective hole masses exhibiting a large spread from $0.3m_0$ in cubic HfO_2 to $8.3m_0$ in tetragonal HfO_2. The conduction band electrons have effective masses of roughly identical order, the heaviest of $1.97m_0$ and the lightest one of $0.68m_0$, being observed in the case of cubic HfO_2.

In the cubic modification of HfO_2 for the conduction band bottom at the Γ point, there is a doubly degenerated state that splits along the Γ-X direction, being preserved in the Γ-L direction. In tetragonal HfO_2 the top of the valence band is degenerated, the degeneration being preserved in the directions A-M and Z-A. The conduction electrons are light in both directions. In monoclinic HfO_2 the electronic states are nondegenerated for both the valence band top and the conduction band bottom.

Figures 12–14 show the PDOS predicted for the $4f$, $5p$, and $5d$ orbitals of Hf and for the $2s$ and $2p$ orbitals of O for the cubic, tetragonal, and monoclinic modifications of HfO_2. The contribution of the $6s$ orbital of Hf to the electron density is negligible, and its partial contribution to DOS is not

TABLE III. Effective electron and hole masses in the atomic units for cubic, tetragonal, and monoclinic HfO_2.

Crystallographic direction	Crystallographic				
	m_{h1}/m_0	m_{h2}/m_0	direction	m_{e1}/m_0	m_{e2}/m_0
		Cubic HfO_2			
Γ-X	0.32	···	L-Γ	0.86	0.86
X-W	3.04	···	Γ-X	1.97	0.68
		Tetragonal HfO_2			
Z-A	0.78	0.78	M-Γ	0.72	···
A-M	8.26	8.26	Γ-Z	0.94	···
		Monoclinic HfO_2			
Z-Γ	0.85	···	A-B	1.03	···
Γ-Y	1.28	···	B-D	1.21	···

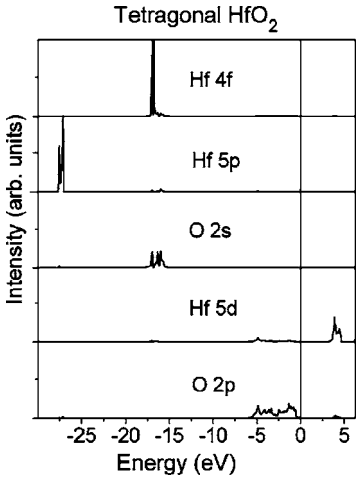

FIG. 13. Partial densities of the states due to 4*f*, 5*p*, and 5*d* orbitals of Hf and of those due to 2*s* and 2*p* orbitals of O in tetragonal HfO_2.

shown in the figure. It can be seen that the relative contributions of the various orbitals to the density of states for the three modifications are roughly identical.

It is further realized that, like most of the transition-metal oxides, the density of states in the conduction band of HfO_2 is made up by the *d* states of the transition metal, i.e., by the Hf 5*d* orbitals.[5,6] The 5 eV wide upper subband of the valence band is formed mainly by the 2*p* electron states of oxygen with partially Hf 5*d* states. The intermediate subband, of 2 eV width, is formed by Hf 4*f* states with some O 2*s* states. Note that the peak due to the Hf 4*f* orbital in the figure is truncated as the actual intensity of the peak is five times larger. The lower narrow subband, 0.1 eV wide, is almost completely formed by the Hf 5*p* states.

The calculated total density of states agrees well with the valence band photoelectron spectrum (see Figs. 6 and 12–14). There are three subbands separated by ionic gaps. It is noted that the difference between the width of the predicted TDOS peaks (the two lower peaks have half-widths of 1.5 and 2.5 eV) and the width of the corresponding experimental peaks (half-width of 5 eV) is quite large. This discrepancy can be attributed to the finite lifetime of holes at the core levels which results in the broadening of the peaks in experimental spectra. However, taking into account the processes resulting in peak broadening (Auger processes, for instance) would require a more precise theoretical model and is out of the scope of the present study.

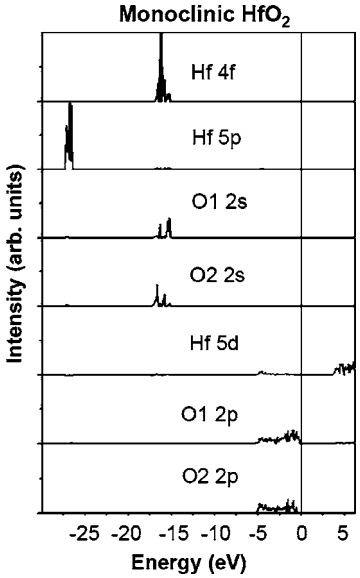

FIG. 14. Partial densities of the states due to 4*f*, 5*p*, and 5*d* orbitals of Hf and due to 2*s* and 2*p* orbitals of three-coordinated O1 and four-coordinated O2 in monoclinic HfO_2.

IV. CONCLUSIONS

In summary, the band structures of the cubic, tetragonal, and monoclinic polymorphous modifications of HfO_2 have been calculated with DFT. The results agree with the experimental photoelectron spectroscopy data. The valence band of HfO_2 consists of three subbands separated from each other by ionic gaps. The upper subband is formed by O 2*p*, Hf 4*f*, and Hf 5*d* states; the intermediate subband is formed by O 2*s* and Hf 4*f* states, whereas the lower narrow subband is mainly formed by Hf 5*p* states. We calculate the effective electron and hole masses in HfO_2. The effective electron masses for different directions in the Brillouin zone fall into the interval of $0.2m_0-2.0m_0$. The calculations show that there exist heavy and light holes for various directions in the Brillouin zone for all the three modifications. The pronounced anisotropy of the electron and hole masses suggests that charge injection into Si may be effectively suppressed by growing a certain orientation crystalline HfO_2 film. Those effects would have significant impact on the current conduction over the dielectric films.[34] The present calculations are based on bulk material structure. The results should be partially applicable to ultrathin (~2 nm) film where the effect of interfacial layer and the interface bonding must be taken into account.[8,34] The crystallization effects, the fluctuation of effective masses, the anisotropy of electron, and the hole masses should still exist in the ultrathin films.

ACKNOWLEDGMENTS

The authors would like to thank Dr. A. V. Shaposhnikov for fruitful discussions and Dr. V. Filip for his help in proofreading this paper. This work was supported by a grant from the Siberian Division of the Russian Academy of Sciences (Grant No. 97), RFBR No, 06-02-16621, a UGC Competitive Earmarked Research Grant of Hong Kong (Project No. CityU 1167/03E), and the National Program for Tera-Level Nanodevice funded by the Korean Ministry of Science and Technology.

[1] V. A. Gritsenko, *Atomic and Electronic Structure of Amorphous Dielectrics in MOS structures* (Nauka, Novosibirsk, 1993).
[2] V. A. Gritsenko, *Silicon Nitride in Electronics* (Elsevier, New York, 1988).
[3] K. Hirose, H. Nohira, T. Koike, K. Sakano, and T. Hattori, Phys. Rev. B **59**, 5617 (1999).
[4] G. D. Wilk, R. M. Wallace, and J. M. Anthony, J. Appl. Phys. **89**, 5243 (2001).
[5] H. Wong and H. Iwai, Microelectron. Eng. **83**, 1867 (2006).
[6] G. Bersuker, P. Zeitzoff, G. Brown, and H. R. Huff, Mater. Today **26**, 2 (2004).
[7] H. R. Huff, A. Hou, C. Lim *et al.*, Microelectron. Eng. **69**, 152 (2003).
[8] H. Wong, K. L. Ng, N. Zhan, M. C. Poon, and C. W. Kok, J. Vac. Sci. Technol. B **22**, 1094 (2004).

[9]J. Robertson, Eur. Phys. J.: Appl. Phys. **28**, 265 (2004).
[10]V. A. Gritsenko, K. A. Nasyrov, Yu. N. Novikov *et al.*, Solid-State Electron. **47**, 1651 (2003).
[11]V. A. Gritsenko, K. A. Nasyrov, D. V. Gritsenko *et al.*, Semiconductors **39**, 748 (2005).
[12]E. Ruh, H. J. Garret, R. F. Domagala, and N. M. Tallan, J. Am. Ceram. Soc. **4**, 27 (1968).
[13]A. G. Boganov, V. S. Rudenko, and L. P. Makarov, Dokl. Akad. Nauk SSSR **160**, 1065 (1965).
[14]J. P. Holgado, J. P. Espinos, F. Yubero *et al.*, Thin Solid Films **389**, 34 (2001).
[15]J. Aarik, A. Aidla, H. Mandar *et al.*, Thin Solid Films **408**, 97 (2002).
[16]R. R. Manory, T. Mori, I. Shimuzu *et al.*, J. Vac. Sci. Technol. A **20**, 549 (2002).
[17]J. Schaefer *et al.*, J. Electrochem. Soc. **150**, 67 (2003).
[18]A. A. Demkov, Phys. Status Solidi B **226**, 57 (2001).
[19]A. S. Foster, F. Lopez Gejo, and A. L. Shluger, Phys. Rev. B **65**, 174117 (2002).
[20]S. M. Sze, *Physics of Semiconductor Devices* (Wiley, New York, 1985).
[21]V. A. Gritsenko, E. E. Meerson, and Yu. N. Morokov, Phys. Rev. B **57**, 2081 (1997).
[22]P. M. Schneider and W. B. Fowler, Phys. Rev. Lett. **36**, 425 (1976).
[23]J. R. Chelikowsky and M. Shluter, Phys. Rev. B **15**, 4020 (1977).
[24]Y.-N. Xu and W. Y. Ching, Phys. Rev. B **23**, 5454 (1981).
[25]S. Zafar, K. A. Conrad, Q. Liu *et al.*, Appl. Phys. Lett. **67**, 1031 (1995).
[26]N. Binsted, J. W. Campbell, and S. J. Gurman, SERC Daresbury Laboratory, EXCURVE92 program, 1991 (unpublished).
[27]V. V. Afanas'ev, A. Stesmans, and F. Chen, Appl. Phys. Lett. **81**, 1053 (2002).
[28]W. J. Zhu and T. P. Ma, IEEE Electron Device Lett. **23**, 597 (2002).
[29]J. Wang, H. P. Li, and R. Stivens, J. Mater. Sci. **27**, 5397 (1992).
[30]G. B. Bokiy, *Introduction into Crystallochemistry* (Moscow State University, Moscow, 1954).
[31]BAND2004.01, SCM, Theoretical Chemistry, Vrije Universiteit, Amsterdam, The Netherlands, http://www.scm.com
[32]G. te Velde and E. J. Baerends, Phys. Rev. B **44**, 7888 (1991).
[33]G. Wiesenekker and E. J. Baerends, J. Phys.: Condens. Matter **3**, 6721 (1991).
[34]H. Wong and H. Iwai, J. Vac. Sci. Technol. B **24**, 1785 (2006).